# Constitutive Laws with Damage Effect for the Human Great Saphenous Vein

Wenguang Li

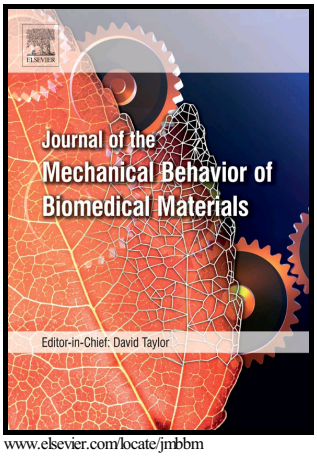


www.elsevier.com/locate/jmbbm

PII: S1751-6161(18)30214-5
DOI: https://doi.org/10.1016/j.jmbbm.2018.02.027
Reference: JMBBM2704

To appear in: *Journal of the Mechanical Behavior of Biomedical Materials*

Received date: 13 November 2017
Revised date: 13 February 2018
Accepted date: 22 February 2018

Cite this article as: Wenguang Li, Constitutive Laws with Damage Effect for the Human Great Saphenous Vein, *Journal of the Mechanical Behavior of Biomedical Materials,* https://doi.org/10.1016/j.jmbbm.2018.02.027

# Constitutive Laws with Damage Effect for the Human Great Saphenous Vein

Wenguang Li

School of Mathematics & Statistics, University of Glasgow, Glasgow, G12, 8QQ, UK

Wenguang.Li@Glasgow.ac.uk



Current date: 22/02/2018

## Abstract

Strain energy-based constitutive laws with damage effect were proposed by using existing both uniaxial tensile test and tubular biaxial inflation test data on the human great saphenous vein (GSV) segments. These laws were applied into GSV coronary artery bypass grafts (CABG) by employing a thin-walled vessel model to evaluate their passive biomechanical performance under coronary artery physiological conditions at a fixed axial pre-stretch. At a peak systolic pressure in 100-150mmHg, a 20-33% GSV diameter dilation was predicted with the law based on tubular biaxial inflation test data and agreed well with 25% dilation in clinical observation in comparison with as small as 2-4% dilation estimated with the law based on uniaxial tensile test data. The constitutive law generated by tubular biaxial inflation test data was mostly suitable for GSV CABG under coronary artery physiological conditions than that based on uniaxial tensile test results. With these laws, the fibre ultimate stretch was extracted from uniaxial tensile test data and the structural sub-failure/damage threshold of 1.0731 was decided for the human GSV. GSV fibres could exhibit damage effect but unlikely undergo a structure failure/break, suggesting a damage factor might exist during CABG arterialization. The damage in GSV tissue might initiate or contribute to early remodelling of CABG after implantation.


Keywords: Great saphenous vein, Constitutive law, Damage model, Coronary artery bypass graft, Strain energy function, Collagen fibre orientation

# 1 Introduction

The great saphenous vein (GSV) is a large, subcutaneous, superficial vein of the human leg. The vein runs along the length of the lower limb, see Fig. 1(a). A healthy human GSV wall consists of three layers, namely intima, media and adventitia from inner to outer surface of the wall [3-6]. Generally, the intima is thin as 60.07μm±1.12, composed of endothelium and an internal elastic lamina next to the media. The media mean thickness is 360.54μm±4.56, in which there are longitudinally orientated smooth muscle cells next to the intima and circular smooth muscle cells next to the adventitia. The two smooth muscle layers are separated by collagen fibres. The adventitia is full of collagen fibres with some fibroblasts and capillaries as well as longitudinally orientated smooth muscle cells [6]. Presently, there is little information about collagen fibre orientation and dispersion in the human GSVs. A mean fibre orientation of $37\pm6^{o}$ against the circumferential direction in the media [7] was observed in comparison with $40^{o}$ in the media of porcine vascular tissues (including vena cava, abdominal aorta and iliac artery) [8]. In the adventitia of the porcine vascular tissues, the fibre mean orientation was $60^{o}$ from the circumferential direction [8].

A segment of GSV can be harvested and utilized to connect the blocked coronary artery and the aorta to build a bypass duct, see Fig.1(b), consequently the blood can stream into the coronary artery again to make the arrested heart recovery. The idea that the human GSV is used clinically as a coronary artery bypass graft (CABG) can be traced back to 1930's [9]. However, the direct coronary artery surgery by using CABG technique began in 1968 in the USA actually [10]. Presently, coronary artery disease (CAD) is a main cause of mortality worldwide. In England, for example, NHS carries out nearly 20,000 CABGs every year [11].

After CABG surgery, GSV CABG has to undergo an arterialization process. In the process, unfortunately, GSV CABGs remodel and develop various diseases, such as aneurysms, thrombosis, atherosclerosis and fibro-intimal hyperplasia, which are associated with smooth muscle cells and extracellular matrix [12-15]. In the first post-surgery month, 13-14% of CABGs occlude because of thrombosis. By the end of the first year of the surgery, intimal hyperplasia develops to reduce graft diameter by 25-30%. In the following years, grafts occlude at a rate of 2% per year as intimal hyperplasia develops. Beyond 5 years, vein grafts are in atherosclerosis due to necrosis, haemorrhage, calcification, and thrombosis [16]. The remodelling, disease and failure are related closely to physiological haemodynamic conditions in the contrary artery [16] and passive biomechanical properties of GSV such as compliance [17].

Some attention has been paid to passive biomechanical properties of GSV by using experiment *in vitro* since 1960's. These experimental contributions can be divided into four categories: (1) global property constant measurements, such as compliance [18-20], pressure-diameter relationships [21-23] and circumferential and longitudinal incremental Young's moduli [24] by making use of vessel segment inflation method and an incremental Young's modulus by bugle

method [25]; (2) ultimate stress and strain as well as stiffness etc. by using uniaxial tensile test on circumferential and longitudinal specimens [26, 27]; (3) stress-strain curves with uniaxial tensile test on circumferential and longitudinal specimens [28, 29]; (4) biaxial stress-strain curves measured by using vessel segment inflation approach [30-32]. These experimental results have provided a valuable basis for further investigations. Importantly, a micro-fibrillary damage could be observed in GSV tissue under a low intraluminal pressure, namely in a range of 50-60mmHg [28].

Compliance mismatch between a GSV CABG and the coronary artery can degrade the graft performance and result in a loss of patency, which is the degree of openness of a vessel, in term of time after surgery [33]. Compliance of GSV can be correlated to CABG patency [34]. Incremental Young's modulus, ultimate stress and strain, stiffness, and stress-strain curves, however, haven't found any clinical applications in CABGs presently.

Under coronary artery haemodynamic conditions, GSV CABG will be subject to an intraluminal pressure as high as 100-150mmHg [35], how the deformation of GSV CABG to develop in this condition and the corresponding levels of stress and strain/stretch are of vital important to understanding of its actual working situation and mechanisms for its remodelling and disease occurrence from a biomechanics point of view. Unfortunately, this issue has not been addressed; further, the micro-fibrillary damage observed in GSV tissue under an intraluminal pressure as low as 50-60mmHg [28] has not been included in constitutive laws of GSV in literature so far.

In the paper, it is attempted to develop constitutive laws of GSV by involving with collagen fibre orientation dispersion and micro-fibrillary damage effect based on stress-strain/stretch data obtained by uniaxial tensile test and vessel segment inflation test, i.e. tubular biaxial inflation test found in literature. Then these constitutive laws are applied into coronary artery haemodynamic conditions to predict the stress and stretch levels of CABG by employing a thin-walled vessel model. Thirdly, the suitability of these constitutive laws for coronary artery physiological environment is evaluated against clinical observations on post-surgery CABG diameter. Finally, micro-fibrillary damage threshold and hypothesis on the reason why GSV remodels are proposed and discussed. These constitutive models and the established method for determining model constants could be meaningful in biomedical engineering and clinical application.



## 2 Constitutive Laws for GSVs

### 2.1 Experiment data adopted

The specimens harvested from human GSV segments in the longitudinal/axial direction and the cut ring from the segments along the circumferential/transverse direction were stretched by using uniaxial tensile test method on an ordinary material testing machine in [29]. The specimens and patients information are tabulated in Table 1. Even though the experiment was made on five pairs of specimens (circumferential and longitudinal), just four specimen pairs were tested successfully, thus

the information of these four pairs is listed and the pair name are kept the same as in [29] in the table. The experimental details are referred to [29]. The experimental circumferential and longitudinal Cauchy stress-stretch curves, such as $\sigma_c^{\exp}$ - $\lambda_c^{\exp}$ and $\sigma_l^{\exp}$ - $\lambda_l^{\exp}$, are plotted in Fig. 2(a) for the specimens in Table 1.

Usually, the harvested GSV segment is distended manually with a pressure before CABG surgery to improve its patency. Two tubular biaxial inflation tests, one is for a normal GSV vessel segment, and one for a GSV segment with manual pressure distension in a range of 250-300mmHg, were carried out in [30] to clarify the effects of manual distension with a maximum internal pressure 140cm$H_2O$ (103mmHg or 13.7kPa). The second Piola-Kirchhoff stress-Green strain curves in [30] were converted into the Cauchy stress-stretch curves.

Three vessel segment inflation tests were conducted on the human GSV segments [31] with 4kPa (30mmHg) pressure increment in four time-steps to achieve 16kPa (120mmHg) systolic pressure. The Cauchy stress-stretch curves have been provided in [31]. The data in Case A where the segment was loaded with a quasi-static slow loading rate (0.04Hz) [31] are employed to generate the constitutive law for GSVs. The Cauchy stress-stretch curves of three samples from [30, 31] are presented in Fig. 2(b). SV6 is from [31], while SV7 and SV8 are from [30], their patient information is included in Table 1. The Cauchy stress-stretch curves of SV7 and SV8 are the mean values of the measurements on 12 patients.

The experimental data shown in Fig. 2 will be utilised to establish constitutive laws with damage effect for GSVs in next sections.

## 2.2 The constitutive law with damage effect

Based on the histological evidence in the introduction, GSV walls are composed of three material layers. To simplify the constitutive law, however, the GSV wall is considered as a nonlinear composite material with homogenous matrix and two families of collagen fibre. Both families of fibre are with identical biomechanical property constants, and the same mean fibre orientation angle with respect to the circumferential direction and dispersion parameter, but with opposite spiral developing path on the SGV cylindrical surface. In this case, when there is no any damage during GSV deformation process, the constitutive law can be described by a strain energy function called GOH model proposed in [36]

$$W_{virgin} = \mu\left(I_1 - 3\right) + \frac{k_1}{k_2}\left\{\exp(k_2\left[\kappa I_1 + \left(1-3\kappa\right) I_4 - 1\right]^2) - 1\right\} \tag{1}$$

where $\mu$, $k_1$ and $k_2$ are the material constants, $\kappa$ is the fibre orientation dispersion parameter, $I_1$ is the invariant representing the squared stretch of the tissue, $I_1 = \lambda_c^2 + \lambda_l^2 + \lambda_h^2$, $\lambda_c$ is the circumferential stretch, $\lambda_l$ is the longitudinal stretch, and $\lambda_h$ is the thickness/radial stretch, they yield the

incompressible condition: $\lambda_c\lambda_l\lambda_h=1$, and $I_4$ is the squared stretch along the fibre direction, $I_4=\lambda_c^2\cos^2\beta+\lambda_l^2\sin^2\beta$, $\beta$ is the mean fibre angle.

In [37], the model presented by Eq. (1) was extended into the case where a tissue is subject to damage effect in its deformation process, and applied into the biomechanical property constant identification for animal and human skins. In that case, the strain energy function is written as

$$W_{damage}=\mu\left[(I_1-3)-\frac{(I_1-3)^{m+1}}{(m+1)(\zeta-3)^m}\right]+\frac{k_1}{k_2}\left\{\exp\left(k_2A^2\right)-1-\frac{2k_2A^{n+2}}{(n+2)\left(\xi^2-1\right)^n}\right\} \tag{2}$$

where $A=\lambda_f^2-1$, with $\lambda_f=\sqrt{\kappa I_1+(1-3\kappa)I_4}$ is the fibre stretch, and $m$, $n$, $\xi$ and $\zeta$ are the phenomenological parameters to describe the damage induced material softening. In particular, $m$ and $\zeta$ are associated with the matrix damage; $m$ specifies the sharpness of the stress-stretch curve when damage occurs, and $\zeta$ indicates the value of $I_1$ when the matrix damage occurs, $n$ and $\xi$ are the corresponding parameters for the fibre damage; $n$ is the counterpart of $m$, and $\xi$ demonstrates when the fibres damage occurs in terms of $\lambda_f$. Powers $m$, $n$ are related with the damage dispersion and uniformity of bonds in the tissue. If these parameters are chosen to be $\xi=\zeta=+\infty$ and $m=n=1$, then the GOH model is recovered.

In the paper, the constitutive law, Eq. (2), is adopted to describe the biomechanical properties of GSV wall tissue with damage. The nine model constants, such as $\mu$, $k_1$, $k_2$, $\beta$, $\kappa$, $\zeta$, $m$, $\xi$ and $n$, will be decided based on the uniaxial tensile test data for the specimens harvested along the circumferential and longitudinal directions as shown in Fig. 2(a), and simultaneously those in Fig. 2(b) obtained by tubular biaxial inflation test.

In the uniaxial tensile test of a specimen harvested in the circumferential direction, at an experimental circumferential stretch, $\lambda_c^{\exp}$, there is only one stress component measured, $\sigma_c^{\exp}$. On the other hand, this component can also be computed by using Eq. (2) with a set of temporary nine model constants at $\lambda_c^{\exp}$ in the following manner

$$\sigma_c=\lambda_c\frac{\partial W_{damage}}{\partial I_1}\frac{\partial I_1}{\partial\lambda_c}+\lambda_c\frac{\partial W_{damage}}{\partial I_4}\frac{\partial I_4}{\partial\lambda_c} \tag{3}$$

where $\lambda_t=\lambda_h=1/\sqrt{\lambda_c^{\exp}}$, $I_1=\lambda_c^{\exp 2}+\lambda_t^2+\lambda_h^2$, $I_4=\lambda_c^{\exp 2}\cos^2\beta+\lambda_l^2\sin^2\beta$, $\lambda_t$ and $\lambda_h$ represent the transverse and thickness stretches of the specimen, respectively. Similarly, the stress component of a specimen harvested along the longitudinal direction in the uniaxial tensile test can be computed with the set of temporary nine model constants at $\lambda_l^{\exp}$.

In the tubular biaxial inflation test, the thickness stretch and two invariants should be calculated with the following relationships

$$\lambda_h = 1/\left(\lambda_c^{\exp}\lambda_l^{\exp}\right), I_1 = \lambda_c^{\exp 2} + \lambda_l^{\exp 2} + \lambda_h^2,\ I_4 = \lambda_c^{\exp 2}\cos^2\beta + \lambda_l^{\exp 2}\sin^2\beta \tag{4}$$

Eventually, the nine model constants are then estimated by minimising the objective function with an optimization algorithm at each experimental stretch, $\lambda_c^{\exp}$ and $\lambda_l^{\exp}$ simultaneously:

$$F(\mu, k_1, k_2, \beta, \kappa, \zeta, m, \xi, n) = \sum_{i=1}^{N_c}\left(\sigma_{ci} - \sigma_{ci}^{\exp}\right)^2 + \sum_{i=1}^{N_l}\left(\sigma_{li} - \sigma_{li}^{\exp}\right)^2 \tag{5}$$

where $N_c$ and $N_l$ are the numbers of experimental data for two specimens, respectively, for uniaxial tensile tests, but $N_c = N_l$ for tubular biaxial inflation tests. The optimization process was carried out using *lsqnonlin* function in MATLAB. The approximation between the measurement and the prediction is measured by the standard deviation error at each experimental stretch, $\lambda_c^{\exp}$ and $\lambda_l^{\exp}$:

$$\varepsilon = \frac{1}{\sigma^{mean}}\sqrt{\frac{\sum_{i=1}^{N_c}\left(\sigma_{ci} - \sigma_{ci}^{exp}\right)^2 + \sum_{i=1}^{N_l}\left(\sigma_{li} - \sigma_{li}^{exp}\right)^2}{N_c + N_l}} \tag{6}$$

which is normalised by the arithmetic mean of all experimental stress $\sigma^{mean}$ [37].

After the nine parameters were extracted, the stress–stretch curves of the circumferential and longitudinal specimens in the experimental stretch ranges were predicted, then invariant $I_1$ and fibre stretch $\lambda_f$ values at the ultimate stress in two curves were determined. Finally, the matrix failure invariant $I_{1b}$ is the small one of two $I_1$ values at two ultimate stresses; similarly, the fibre failure stretch $\lambda_{fb}$ is the small one of two $\lambda_f$ values at two ultimate stresses.

### 2.3 Thin-walled vessel model under coronary artery physiological condition

A GSV segment is considered as a thin-walled cylindrical vessel when it is positioned between the aorta and the blocked coronary artery with a constant longitudinal pre-stretch under an internal systolic blood pressure, see Fig. 3. In the circumferential direction, the Cauchy stress caused from the internal pressure is balanced by the circumferential Cauchy stress generated by the GSV wall deformed under this pressure in the plane-strain state, i.e.

$$\frac{rp}{h} = \lambda_c\frac{\partial W_{damage}}{\partial I_1}\frac{\partial I_1}{\partial \lambda_c} + \lambda_c\frac{\partial W_{damage}}{\partial I_4}\frac{\partial I_4}{\partial \lambda_c} \tag{7}$$

where the instant tube radius is $r = \lambda_c r_0$, the instant wall thickness is $h = \lambda_h h_0$, the wall thickness stretch $\lambda_h$ is determined by the material incompressible condition $\lambda_c\lambda_l^{pre}\lambda_h = 1$ with a known pre-stretch, $\lambda_h = 1/\left(\lambda_c\lambda_l^{pre}\right)$, $r_0$ is the initial radius of the vessel, can be calculated by using the perimeter $L$ and the initial wall thickness $h_0$ shown in Table 1. Then $r/h$ in the left hand side of Eq. (7) can be

expressed with $\lambda_c$, $r_0$, $h_0$ and $\lambda_l^{pre}$, such as $r/h = r_0\lambda_l^{pre}\lambda_c^2/h_0$, and eventually, Eq. (7) can be written as

$$\frac{pr_0\lambda_l^{pre}\lambda_c^2}{h_0} = \lambda_c\frac{\partial W_{damage}}{\partial I_1}\frac{\partial I_1}{\partial \lambda_c} + \lambda_c\frac{\partial W_{damage}}{\partial I_4}\frac{\partial I_4}{\partial \lambda_c} \tag{8}$$

where the internal systolic blood pressure $p$ increases linearly from zero to a maximum pressure $p_{\max}$, here $p_{\max}$ =250mmHg. At each pressure, the corresponding circumferential stretch $\lambda_c$ can be solved from Eq. (8) based on the known constitutive law by minimizing the difference between the terms in both the sides of Eq. (8) in the MATLAB (*lsqnonlin* function). After the circumferential stretch $\lambda_c$ is determined, the longitudinal stress is calculated with the following equation

$$\sigma_l = \lambda_l^{pre}\frac{\partial W_{damage}}{\partial I_1}\frac{\partial I_1}{\partial \lambda_l}\bigg|_{\lambda_l=\lambda_l^{pre}} + \lambda_l^{pre}\frac{\partial W_{damage}}{\partial I_4}\frac{\partial I_4}{\partial \lambda_l}\bigg|_{\lambda_l=\lambda_l^{pre}} \tag{9}$$

Finally, the fibre and matrix stretches and stresses at each $p$ are obtained, and in turn, the biomechanical performance of a GSV CABG under coronal artery physiological conditions can be assessed.

# 3 Results

## 3.1 Constitutive laws from uniaxial tensile tests

The model constants of constitutive law for four GSV samples such as SV2-5 are illustrated in Table 2 and a comparison of the Cauchy stress-stretch curves predicted with these constants is made in Fig. 4 against the experimental data of SV2-5. Generally, the stress-stretch curves predicted with the constitutive law with damage effect and extracted model constants are good agreement with the experimental measurements in the maximum error of 6.04% and the minimum error of 1.31%.

Since the longitudinal stress-stretch curve is stiffer than the circumferential stress-stretch curve, the mean fibre angle $\beta$ is bigger than $50^o$ for all the samples, resulting in a mean fibre angle of $57.2^o$.

The matrix material stiffness $\mu$ shows a less variation in GSV groups with a mean of 0.22MPa. The initial fibre stiffness $k_1$ demonstrates a little variation across the samples with 5.86MPa mean value. The fibre stiffness incremental rate $k_2$, and damage related parameter $m$ show a significant change across the samples, but the rest parameters remain less varied from one sample to another.

The ultimate matrix invariant $I_{1b}$ and fibre stretch $\lambda_{fb}$, which are defined as the matrix invariant and fibre stretch values at which the sample/specimen structure fails in a uniaxial tensile test, remain nearly unchanged across specimens. Their mean values are 4.0451 and 1.1442, respectively.

The ultimate Cauchy stresses $\sigma_{lb}$ and $\sigma_{cb}$ are the largest level of the stresses in GSV samples in the circumferential and longitudinal directions, respectively. Their mean values are 5.32MPa in the longitudinal direction and 2.5142MPa in the circumferential direction, respectively.

### 3.2 Constitutive laws from tubular biaxial inflation tests

The determined model constants of constitutive law based on tubular biaxial inflation tests are listed in Table 3 for the human GSV segments SV6-8, and their stress-stretch curves predicted with those constants are demonstrated in Fig. 5 against the experimental data of SV6 to 8. Because a tubular biaxial inflation test can maintain before the segment structure failure occurs only, no ultimate stress and stretch can be extracted from its experimental data.

The $42.46^o$ mean fibre angle optimized is in very good agreement with the $43^o$ prediction in [31] and $37\pm6^o$ measurement in [7]. In comparison with $\mu$ and $k_1$ in Table 2, the two constants for the SV6-8 segments are far too small, suggesting SV6-8 samples are much more compliant than those in Table 2. The rest constants seem comparable with those in Table 2.

### 3.3 Biomechanical performance under coronary artery physiological conditions

SV2, SV3 and SV4 were chosen to clarify its biomechanical response to coronary artery physiological conditions, i.e. intraluminal blood pressures, based on the thin-walled cylindrical vessel model in Section 2.3 because they can cover the whole variation range of experimental stress-stretch curve as shown in Fig.2 (a).

When a GSV segment connects the aorta and the blocked coronary artery as a CABG, the GSV is not in line with the coronary artery, therefore there is no any pre-stretch likely applied on the segment, thus $\lambda_l^{pre}$=1 condition has to be held in the thin-walled vessel model. Note that even though the maximum pressure is given to be 250mmHg, the results within 100-150mmHg systolic peak pressure [35] are interested and discussed here.

The predicted vessel wall stretch, stress and fibre stretch curves are illustrated in Fig. 6 in terms of internal blood pressure for GSV SV2, SV3 and SV4 under coronary artery physiological conditions. The constants presented in Table 2 for SV2 were used in the prediction. Since the longitudinal stretch $\lambda_l$ is kept to be constant, the thickness stretch $\lambda_h$ reduces and the circumferential stretch $\lambda_c$ becomes large with increasing pressure. In the physiological systolic peak pressure range, the CABG shows a little dilation effect ($\lambda_c$=1.022, i.e. 2.2% diameter dilation for SV2 and $\lambda_c$=1.0345, i.e. 3.5% diameter dilation for SV3 and $\lambda_c$=1.0190, i.e. 1.9% diameter dilation for SV4), which is much smaller than a 25% diameter dilation observed after a week of CABG surgery completed [39]. This suggests that the stress-stretch curve predicted by using the constitutive law based on uniaxial tensile test data is too stiff in the physiological systolic peak pressure condition, and the law is unsuitable for this condition.

The level of longitudinal Cauchy stress is higher than the circumferential stress in the physiological systolic peak pressure range, but these levels are far below the ultimate stresses measured on the human GSVs [26, 27] and those shown in Fig. 2(a). This effect suggests that there is a little risk of tissue structural failure from a stress point of view based on the constitutive law determined with uniaxial tensile test data.

The fibre stretch $\lambda_f$ rises with increasing internal pressure in Fig. 6(c), and whatever the level of fibre stretch is, $\lambda_f$ is always far below the fibre ultimate/break stretch $\lambda_{fb}$. In the figure, a fibre stretch threshold for damage determined, which is based on the threshold of intraluminal pressure in the range 50-60mmHg for the human GSVs [28], i.e. $\lambda_{fd}$=1.0731, is involved as well. Obviously, fibre damage/sub-failure doesn't occur. The same situation is held for the matrix failure invariant $I_{1b}$ as shown in Fig. 6(d). These two facts indicate that there are no substructure damage and failure in the tissue from a stretch/strain point of view.

Next, SV6 was chosen to be a CABG and its constitutive law determined with tubular biaxial inflation test data shown in Table 3 was applied into the coronary artery physiological condition with the same pressure range and initial vessel geometry as SV2. The corresponding stretch-, stress-, fibre stretch- and invariant $I_1$-pressure curves are illustrated in Fig. 7. It is seen that $\lambda_c$ has reached 1.2 as soon as the internal pressure increases to 8.5mmHg, and then keeps slowly rising to 1.335 until 150mmHg, showing a 20-33% remarked dilation in vessel diameter. This dilation value agrees well the observation of 25% [39]. This implies that the stress-stretch curve predicted by using the constitutive law based on tubular biaxial inflation test data is suitable for the physiological systolic peak pressure condition.

For the circumferential and longitudinal stresses, since the mean fibre angle is less than $45^o$, the circumferential stress is higher than the longitudinal one in magnitude. Furthermore, the level of two stresses is much lower than the ultimate stress shown in Table 2 and Fig. 2(a).

The fibre stretch $\lambda_f$ is plotted in Fig. 7(c), and the mean fibre ultimate stretch $\lambda_{fb}$=1.1442 based on the data in Table 2 is provided. Additionally, the fibre damage stretch $\lambda_{fd}$=1.0731 for the human GSV [28] is involved. Clearly, the fibre stretch has been beyond the damage threshold as $p \geq$ 8mmHg, but always below the ultimate stretch. This fact suggests that the GSV can be damaged but its structure is not broken under coronary artery physiological conditions, and the tissue will be subject to remodelling along with wall thickening effect.

The invariant $I_1$ is still lower than the failure invariant $I_{1b}$, see Fig. 7(d), confirming there is no structure failure under coronary artery physiological conditions. Unfortunately, there is no matrix material threshold for damage; we are unable to predict whether there is a damage effect in the matrix.

### 3.4 Effect of manual pressure distension

The established two constitutive laws based on two tubular biaxial inflation tests for the normal GSV segment and the GSV segment with manual pressure distension in 140cm $H_2O$ [30] in Table 3 are applied to the GSV CABG thin-walled vessel model respectively as done in Section 3.3 to identify CABG responses to coronary artery physiological pressures. The results for SV7 and 8 as indicated by 'normal, and 'distended' are illustrated in Fig. 8 in terms of internal pressure. It is shown that the GSV segment with manual pressure distension is less expanded ($\lambda_c$ =1.1605 at 150mmHg), lower stress level and shorter fibre stretch.

This suggests that manual pressure distension can be favourable to suppress GSV segment dilation. However, such distension can induce structural and functional damage to the endothelium of GSV segment; hence, this technique should be applied with caution.

## 4 Discussions

In the paper, an analytical approach is proposed to handle experimental data in uniaxial tensile test or tubular biaxial inflation test on GSV segments and then the corresponding constitutive laws with sub-failure/damage effect are established, eventually they are applied into the physiological environment of coronary artery. In consequence, the biomechanical performance of a GSV CABG is evaluated under coronary artery physiological condition before the surgery. This method is significant in biomedical engineering and clinical practice and has not been reported in literature so far.

The mean fibre angle decided by the single layer model above represents an averaged angle of the collagen fibres in the media and adventitia actually. As shown in Table 2 and 3, the mean collagen fibre angle based on uniaxial tensile test results in Section 3.1 is bigger than that based on tubular biaxial inflation test data in Section 3.2 by $20^o$ in average. It was observed that the mean fibre angle in the adventitia is $60^o$ [7] but the angle in the media is $40^o$ [7, 8] resulting in a $20^o$ degree in mean fibre angle between the adventitia and the media. The predicated mean fibre angles agree quite well with these observations.

A uniaxial tensile test shares considerably different stress-stretch regions and curve shapes with a tubular biaxial inflation test for the human GSV segments, as demonstrated in Fig. 9. In uniaxial tensile tests, the specimens are stretched until their complete failure in structure, thus the collagen fibres in the adventitia make a full contribution to the stress-stretch curve. In tubular biaxial inflation tests, however, there is no structure failure at all; consequently the collagen fibres just in the media have a full contribution to the stress-stretch curve, whilst those in the adventitia will take little effect on the curve. Therefore, it is not surprised that the mean fibre angle based on uniaxial tensile test data is bigger than that based on tubular biaxial inflation test results.

In uniaxial tensile tests, the stress-stretch curve measured at low stretch is not as accurate as that at high stretch; as a result, the property constants inversely determined mostly reflect the stiffer biomechanical behaviour of GSV wall at the high stretch. Nevertheless, the constitutive law based on uniaxial tensile test data should result in a less dilatation in GSV diameter under coronary arterial

physiological condition. Thus, such a constitutive law is unsuitable for a GSV CABG working in the coronary artery physiological condition. The most advantage of uniaxial tensile test is nothing more than to provide ultimate stress and stretch of specimens.

In tubular biaxial inflation tests, however, the inflating pressure is in the range of coronary artery physiological pressure; hence, the stress-stretch curve at low stretch is fully exhibited and captured. Consequently, the constitutive law resulted can represent the biomechanical property in the coronary artery physiological condition.

It was observed that a vein graft can experience a >25% increase in lumen in one month due to remodelling after graft surgery [39, 40]. The increase in diameter of GSV segment predicted in the paper as shown in Fig. 7 is in good agreement with this observation. Therefore, the constitutive law with damage effect based on tubular biaxial inflation test data is much more suitable for GSV CABG in comparison with that based on uniaxial tensile test stress-stretch curves.

Remodelling is relevant to blood shear stress independently [41], but only ~10% of luminal remodelling can be explained by shear stress [42]. Here it is supposed that the tissue damage in GSV segment may trigger or contribute significantly to this remodelling process. This hypothesis needs to be confirmed with direct microscopic observation in the future.

When a GSV segment was distended with pressure in a range of 50-60mmHg, micro-fibrillary damage could be observed in [31]. The fibre stretches of SV6 and SV7 at these two pressures have been extracted, and their values are 1.0715 at 50mmHg and 1.0747 at 60mmHg with a mean of 1.0732, which are slightly higher than the sub-failure/damage threshold of rat ligament tissue, $\lambda_{fd}$ =1.0514 observed [43]. An exact sub-failure/damage threshold for the human collagen fibre in GSVs is subject to be updated in the future.

Honestly, the method is subject to a few limitations. Firstly, since GSV wall is thinner than arterial wall, residual strain/stress effect in it may be not significant, and the thin-walled vessel model is adopted. As a result, the residual strain/stress is not taken into account in the model. In the future, the thick-walled model needs to be examined.

In the vessel model, a plane-strain constrain is held to make 3D biomechanics problem be a 2D case for a GSV CABG. This geometrical constrain can result in an additional longitudinal force/stress. This limitation can be removed by solving an additional stress equilibrium equation in the longitudinal direction to obtain a variable longitudinal stretch under different pressures. In this case, the CABG can extend and shrink longitudinally, depending on the mean fibre angle. Whether such a deformation scenario is realistic needs to be confirmed clinically.

As usual, the surrounding tissue effects are considered by a pre-stretch in the model in Section 2.3. The pre-stretch was assigned to be 1 based on Fig. 3 where a GSV seems to be stitched to the aorta and coronary artery simply. Additionally, the surrounding tissue effects can result in stress

concentration actually in the joint of a GSV CABG and the coronary artery induced by surgical suture line. This issue needs to be addressed in the future.

In the paper, the constitutive law developed can describe the consequences of damage but not the damage mechanisms themselves. We only set out characterize what the damage process produces; not attempt to neither identify nor model the damage mechanisms underwent.

It was shown that the damage and failure of soft bio-tissues were layer-specific [44]. GSV fibre failure would exhibit this property. However, because of a lack of microscopy observation on GSV layer failure process, the layer-specific feature in the failure of GSV was not illustrated in the paper.

Failure in the matrix and fibres of a soft tissue can be analysed by using energy limiter method once the constitutive law of the tissue is available. This approach has been proposed and demonstrated extensively in [45-49] and reviewed throughout in [50]. In further articles, this method can be utilised hopefully to interpret the failure mechanism of GSV during uniaxial tensile tests.

Lastly, GSV walls can exhibit viscoelastic effect [51] and the blood pressure in CABG is in pulsation under coronary artery physiological conditions. These two factors remain unconsidered in biomechanical model in Section 2.3. It is hopeful that they can be involved in the model in the future.

Very recently, the biomechanical properties of bovine saphenous [52], jugular [53] venous valve leaflets were measured by using biaxial tensile test method. Further, the passive biomechanical behaviour of jugular venous valves and wall tissues were tested under different biaxial testing protocols, particularly a variable stretch tragedy was adopted in time domain [54]. Against the experimental data, a strain energy function with polynomial and exponential terms was proposed and fitted. These contributions can be significant to bioprosthetic designs and replacement surgeries as well as understanding of venous valvular disease, but also are helpful to CABG design and surgery.

## 5 Conclusions

In the paper, constitutive laws with damage effect based on a strain energy function were developed by using existing either uniaxial tensile test data on specimens harvested from the human GSV segments longitudinally and circumferentially or tubular biaxial inflation test results on GSV segments. The GSV segments were considered as a composite of homogenous matrix and anisotropic two families of collagen fibre; and the nine model constants in the laws are determined inversely with MATLAB codes. The matrix and fibre structural failure indices such as ultimate/break stress and stretch were also extracted from uniaxial tensile test data.

The GSV segments with these constitutive laws were loaded with a series of pressures at a certain pre-stretch by employing a thin-walled vessel model to identify the GSV biomechanical performance in coronary artery physiological environment. It turned out that the dilation of GSV CABG diameter was just 2.2% based on the constitutive law decided with uniaxial tensile test data, which was far below clinical observation. However, the dilation predicted by the constitutive law

determined with tubular biaxial inflation test data could be as high as 33% under the coronary artery physiological condition, showing good agreement with the observation and suggesting this constitutive law is suitable for the human GSV wall.

With this law and the human GSV structural sub-failure/damage thresholds were decided. A fibre stretch in 1.0715-1.0747 may be a good approximation to the sub-failure/damage threshold for human collagen fibre in GSVs. It was found that the fibre stretch had been over the threshold as soon as the pressure was larger than 8mmHg, and GSV fibres could be in damage state but unlikely experienced a complete structure failure/break in terms of ultimate stress and stretch. The matrix structure didn't seem to break as well; however, whether it is in sub-failure/damage situation needs to be convinced with microscopic observations. Tissue damage in GSV wall may trigger or play an important role in remodelling process.

Further work includes fibre and matrix material sub-failure/damage microscopic observation and threshold confirmation, thick-walled vessel model examination and residual strain effect consideration.

## Compliance with Ethical Standards:

Funding: This study was not funded by anybody.

Conflict of Interest: The author has no conflict of interest.

Ethical approval: This article does not contain any studies with human participants or animals performed by the author.

## References

[1] http://www.surgery.usc.edu/vascular/varicoseveinsandvenousdisease.html

[2] https://atlasofscience.org/a-novel-treatment-for-saphenous-venous-graft-thrombosis/

[3] Spary T L and Roberts W C, Changes in saphenous veins used as aortocoronary bypass grafts, Fundamentals of Clinical Cardiology, 1977, 94:500-516.

[4] Thine G, Miazzi P, Valsecchi M, Valente M, Bortolotti U, Casarotto D and Gallucci V, Histological survey of the saphenous vein before its use as autologous aortocoronary bypass graft, Thorax, 1980, 35:519-522.

[5] Milroy C , Scott D J A, Beard J D, Horrocks M and Bradfield W B, Histological appearance of the saphenous vein, Journal of Pathology, 1989, 159:311-316.

[6] Naim M M and Elsharawy M, Histological assessment of the long saphenous vein in normal and varicose veins, The Egyptian Journal of Histology, 2005, 28:281-290.

[7] Vesely J, Hadraba D, Chlup H, Horny L, Adamek T and Zitny, Constitutive modelling and histological of vena saphena, Applied Mechanics and Materials, 2014, 486:249-254.

[8] Snowhill P B and Silver F H, A mechanical model of porcine vascular tissues-Part I: determination of macromolecular component arrangement and volume fractions, Cardiovascular: An International Journal, 2005, 4:281-294.

[9] Diodato Ml and Chedrawy E G, Coronary Artery Bypass Graft Surgery: The Past, Present, and Future of Myocardial Revascularisation, DOI:http://dx.doi.org/10.1155/2014/726158.

[10] Miller D W and Dodge H T, Benefits of coronary artery bypass surgery, Archives of Internal Medicine, 1977; 137:1439-1446.

[11] http://www.nhs.uk/conditions/Coronary-artery-bypass/Pages/Introduction.aspx

[12] Hassantash S A, Bikdeli B, Kalantarian S, Sadeghian M and Afshar H, Pathophysiology of aortocoronary saphenous vein bypass graft disease, Asian Cardiovascular & Thoracic Annals, 2008; 16(4):331-336.

[13] Vlodaver Z and Edwards J E, Pathologic changes in aortic-coronary arterial saphenous vein grafts, Circulation, 1971; 44:719-728.

[14] Walts A E, Fishbein M C, Sustaita H and Matloff J M, Ruptured atheromatous plaques in saphenous vein coronary artery bypass grafts: a mechanism of acute, thrombotic, late graft occlusion, Circulation, 1982; 65:197-201.

[15] Ramirez F D, Hibbert B, Simard T, Pourdjabbar A, Wilson K R, Hibbert R, Kazmi M, Hawken S, Ruel M, Labinaz M and O'Brien E R, Natural history and management of aortocoronary saphenous vein graft aneurysms, Circulation, 2012; 126:2248-2256.

[16] de Vries M R, Simons K H, Jukema J W, Braun J and Quax H A, Vein graft failure: from pathophysiology to clinical outcomes, Nature Reviews, 2016; 13:451-470.

[17] Zachrisson H, Lindenberger M, Hallman D, Ekman M, Neider D and Lanne T, Diameter and compliance of the greater saphenous vein-effect of age and nitro-glycerine, clinical Physiology and Functional Imaging, 2011; 31:300-306.

[18] Khalil A, El-Bayar M and Molokhia F, Dispensability of isolated segments of femoral and saphenous veins, Angiology, 1968, 19(7): 419-422.

[19] Bocking J K and Roach M R, The elastic properties of the human great saphenous vein in relation to primary varicose veins, Canadian Journal of Physiology and Pharmacology, 1974, 52:153-157.

[20] Walden R, L'Italien G J, Megerman J and Abbott W M, Matched elastic properties and successful arterial grafts, Archives of Surgery, 1980, 115: 1165-1169.

[21] Angelini G D, Passani S L, Breckenridge I M and Newby A C, Nature and pressure dependence of damage induced by distension of human saphenous vein coronary artery bypass grafts, Cardiovascular Research, 1987, 21:902-907.

[22] Stooker W, Gok M, Sipkema P, Niessen H W M, Baidoshvili A, Westerhof N, Jansen E K, Wildevuur C R H and Eijsman L, Pressure-diameter relationship in the human greater saphenous vein, Annals of Thoracic Surgery, 2003, 76:1533-1538.

[23] Paranjothi K, Saravanan U, KrishnaKumar R and Balakrishnan K R, Mechanical Properties of Human Saphenous Vein, Mechanics of Biological Systems and Materials-Volume 2, New York: Springer 2011: 79-85.

[24] Wesly R L R, Vaishnav R N, Fuchs J A, Patel D J and Greenfield C, Static linear and nonlinear elastic properties of normal and arterialized venous tissue in dog and man, Circulation Research, 1975, 37:509-520.

[25] Forouzandeh F, Bozorgi M H, Meshkat B and Fatouraee N, Measurement of mechanical properties of human saphenous vein using an inflation experiment, Proceedings of 20th Iranian Conference on Biomedical Engineering, Tehran, Iran, December 18-20, 2013.

[26] Psaila J V and Mehuish J, Viscoelastic properties and collagen content of the long saphenous vein in normal and varicose veins, British Journal of Surgery, 1989, 76, 37-40.

[27] Donovan D L, Schmidt S P, Townshend S P, Njus G O and Sharp W V, Material and structural characterization of human saphenous vein, Journal of Vascular Surgery, 1990, 12:531-537.

[28] Ozturk N, Sucu N, Comelekoglu U, Yilmaz B C and Aytacoglu B N, Pressure applied during surgery alters the biomechanical properties of human saphenous vein graft, Heart Vessels, 2013, 28:237-2245.

[29] Hamedani B A, Navidbakhsh M and Tafti H A, Comparison between mechanical properties of human saphenous vein and umbilical vein, BioMedical Engineering Online, 2012;11:59-74.

[30] Zhao J B, Andersen J J, Yang J, Rasmussen B S, Liao D H and Gregersen H, Manual pressure distension of the human saphenous vein changes its biomechanical properties-implication for coronary artery bypass grafting, Journal of Biomechanics, 2007, 40:2268-2276.

[31] Vesely J, Horny L, Chlup H and Zitny R, Inflation tests of vena saphena maga for different loading rates, Proceedings of 13th Mediterranean Conference on Medical and Biological Engineering and Computing, Roa Romero L. (eds) Vol. 41. Springer, Cham, 2014, 1041-1044.

[32] Vesely J, Horny L, Chlup H, Adamek T, Krajicek M and Zitny, Constitutive modelling of human saphenous veins at overloading pressures, Journal of the Mechanical Behavior of Biomedical Materials, 2015, 45:101-108.

[33] Abbott W M, Megerman J, Hasson J E, L'Italien G and Warnock D F, Effect of compliance mismatch on vascular graft patency, Journal of Vascular Surgery, 1987, 5(2): 376-382.

[34] Salacinski H J, Goldner S, Giudiceandrea A, Hamilton G and Seifalian A M, The mechanical behaviour of vascular grafts: a review, Journal of Biomaterials Applications, 2001, 15: 241-278.

[35] Siogkas P K, Papafaklis M I, Sakellarios A I, Stefanou K A, Bourantas C V, Athanasiou L S, Exarchos T P, Naka K K, Michalis L K, Parodi O and Fotiadis D I, Patient-specific simulation of coronary artery pressure measurements: An in vivo three-dimensional validation study inhuman, BioMed Research International, 2015, http://dx.doi.org/10.1155/2015/628416.

[36] Gasser T, Ogden R and Holzapfel G, Hyperplastic modelling of arterial layers with distributed collagen fibre orientations, Journal of the Royal Society Interface, 2006, 3:15-35.

[37] Li W G and Luo X Y, An invariant-based damage model for human and animal skins, Annals of Biomedical Engineering, 2016; 44:3109-3122.

[38] https://www.slideshare.net/drdrsingh06/cabg-on-cpb.

[39] Gasper W J, Owens C D, Kim J M, Hills N, Belkin M, Creager M A and Conte M S, Thirty-day vein remodeling is predictive of midterm graft patency after lower extremity bypass, Journal of Vascular Surgery, 2013, 57: 1-18.

[40] Dobrin P B, Littooy F N, Golan J, Blakeman B and Fareed J, Mechanical and histologic changes in canine vein grafts, Journal of Surgical Research, 1988, 44:259-265.

[41] Gusicc R J, Myung R, Petko M, Gaynor J W, Gooch K J, Shear stress and saphenous vein remodeling ex vivo, Journal of Biomechanics, 2005, 38: 1760-1769.

[42] Owens C D, Gasper W J, Rahman A S and Conte M S, Vein graft failure, Journal of Vascular Surgery, 2015, 61: 203-216.

[43] Provenzano P P, Heisey D, Hyashi K, Lakes R and Vanderby R, Subfailure damage in ligament: a structure and cellular evaluation, Journal of Applied Physiology, 2002, 92:362-371.

[44] Volokh K Y, Prediction of arterial failure based on a microstructural bi-layer fiber-matrix model with softening, Journal of Biomechanics, 2008, 41: 447-453.

[45] Volokh K Y, Multiscale modelling of material failure: from atomic bonds to elasticity with energy limiters, International Journal for Multiscale Computational Engineering, 2008, 6(5):393-410.

[46] Volokh K Y and Vorp D A, A model of growth and rupture of abdominal aortic aneurysm, Journal of Biomechanics, 2008, 41:1015-1021.

[47] Trapper P and Volokh K Y, Elasticity with energy limiters for modelling dynamics failure propagation, International Journal of Solid and Structure, 2010, 47:3389-3396.

[48] Volokh K Y, Modeling failure of soft anisotropic materials with application to arteries, Journal of the Mechanical Behavior of Biomedical Materials, 2011, 4:1582-1594.

[49] Volokh K Y, Cavitation instability as a trigger of aneurysm rupture, Biomechanics and Modeling in Mechanobiology, 2015, 14:1071-1079.

[50] Volokh K Y, Review of the energy limiters approach to modelling failure of rubber, Rubber Chemistry and Technology, 2013, 86(3):470-487.

[51] Aisa R, Arezu A M, Nasser F, Saeed S A and Mohammad S, A structural constitutive model for viscoelastic rheological behavior of human saphenous vein using experimental assays, International Journal of Medical, Health, Biomedical, Bioengineering and Pharmaceutical Engineering, 2016, 10(3): 170-173.

[52] Lu J and Huang H S, Biaxial mechanical behavior of bovine saphenous venous valve leaflets, Journal of the Mechanical Behavior of Biomedical Materials, 2018, 77:594-599.

[53] Huang H S and Lu J, Biaxial mechanical properties of bovine jugular venous valve leaflet tissues, Biomechanics and Modeling in Mechanobiology, 2017, 16(6):1911-1923.

[54] Kaul N and Huang H S, Constitutive modeling of jugular vein-derived venous valve leaflet tissues, Journal of the Mechanical Behavior of Biomedical Materials, 2017, 75:50-57.

Table 1 Patient information and GSV specimen specifications

| Contributor | Specimen | Gender | Age | Vessel perimeter $L$ (mm) | Wall thickness $h_0$ (mm) |
|---|---|---|---|---|---|
| Hamedani, Navidbakhsh and Tafti (2012)[29] | SV2 | M | 58 | 13.7 | 0.51 |
| | SV3 | M | 68 | 12.0 | 0.56 |
| | SV4 | F | 57 | 12.3 | 0.53 |
| | SV5 | F | 59 | 11.0 | 0.49 |
| Vesely et al (2014)[31] | SV6 | F | 42 | 17.40 | 0.80 |
| Zhao et al (2007)[30] | SV7 | M(11), F(1) | Mean 67.5(50-81) | 8.64 | 0.85 |
| | SV8 | M(11), F(1) | Mean 67.5(50-81) | 11.31 | 0.90 |

Table 2 Biomechanical property constants for GSV based on uniaxial tensile test

| Constants | SV2 | SV3 | SV4 | SV5 |
|---|---|---|---|---|
| $\mu$ (MPa) | 0.2024 | 0.1670 | 0.1803 | 0.3262 |
| $\beta$ ($^o$) | 54.7244 | 58.5632 | 59.3453 | 56.1022 |
| $\kappa$ (-) | 0.1612 | 0.1915 | 0.1051 | 0.1614 |
| $k_1$ (MPa) | 6.7131 | 4.5020 | 5.8541 | 6.3675 |
| $k_2$ (-) | 35.9777 | 16.7004 | 10.6104 | 0.0033 |
| $\zeta$ (-) | 3.2554 | 3.4988 | 3.8087 | 3.3423 |
| $m$ (-) | 2.4106 | 4.3496 | 9.2480 | 0.9956 |
| $\xi$ (-) | 1.0759 | 1.1043 | 1.1198 | 1.1732 |
| $n$ (-) | 5.1858 | 5.1685 | 3.7541 | 5.1282 |
| $I_{1b}$ (-) | 3.6645 | 3.5677 | 3.7913 | 3.8837 |
| $\lambda_{fb}$ (-) | 1.0959 | 1.1206 | 1.1406 | 1.1363 |
| $\sigma_{cb}$ (MPa) | 2.6250 | 1.6818 | 3.1515 | 2.5985 |
| $\sigma_{lb}$ (MPa) | 5.4260 | 4.8690 | 6.1522 | 4.8458 |
| $\varepsilon$ (%) | 3.6645 | 2.2567 | 5.3814 | 1.7932 |

Table 3 Extracted biomechanical property constants for GSVs based on vessel segment inflation test

| Constants | SV6 | SV7 | SV8 | Remark |
|---|---|---|---|---|
| $\mu$ (MPa) | 0.0008 | 0.0002 | 0.0008 | SV6-Case A in [31]<br>SV7-normal GSV segment without manual pressure distension in [30]<br>SV8-GSV segment with manual pressure distension in [30] |
| $\beta$ ($^o$) | 42.4620 | 35.2191 | 36.7057 | |
| $\kappa$ (-) | 0.2354 | 0.2598 | 0.1719 | |
| $k_1$ (MPa) | 0.0095 | 0.0452 | 0.0114 | |
| $k_2$ (-) | 81.5018 | 128.8342 | 107.7382 | |
| $\zeta$ (-) | 3.4070 | 3.2165 | 3.2240 | |
| $m$ (-) | 8.1224 | 2.5509 | 4.0943 | |
| $\xi$ (-) | 1.0739 | 1.0466 | 1.0692 | |
| $n$ (-) | 5.2274 | 7.0983 | 11.9622 | |
| $\varepsilon$ (%) | 4.0566 | 2.9004 | 2.7813 | |

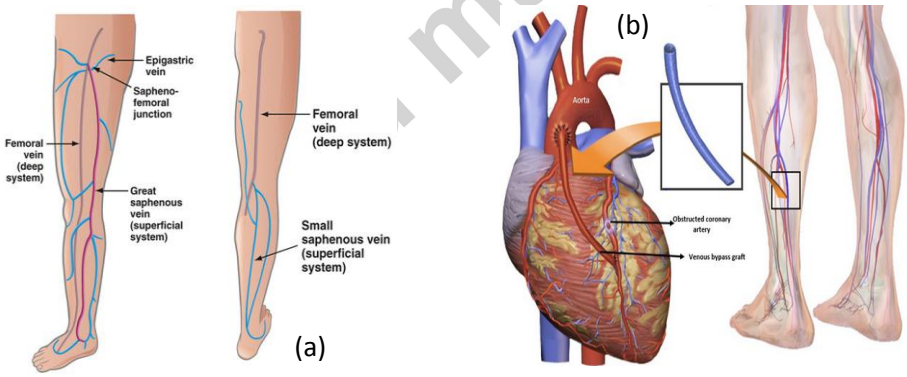


Fig. 1 Greater saphenous vein in human leg (a) and its bypass graft (b), the picture (a) was from [1], the picture (b) was after [2].

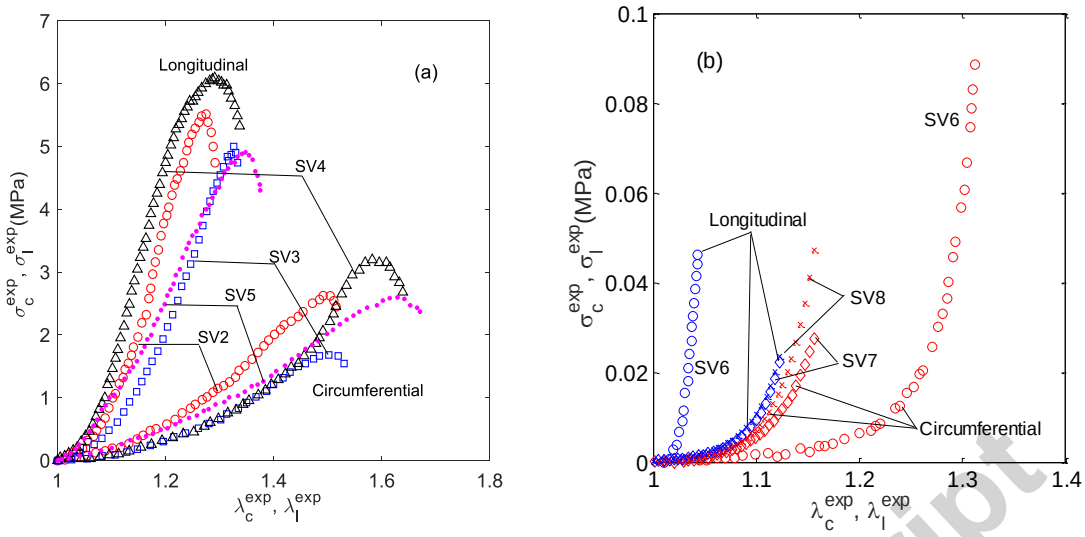


Fig. 2 Measured stress-stretch data of human GSV samples, such as SV2-5 by uniaxial tensile test in [29], SV6 by tubular biaxial inflation test in [31] and SV7 and SV8 by tubular biaxial inflation in [30], SV7-normal condition, SV8-distended manually with a intraluminal pressure of 140cm $H_2O$ [30].

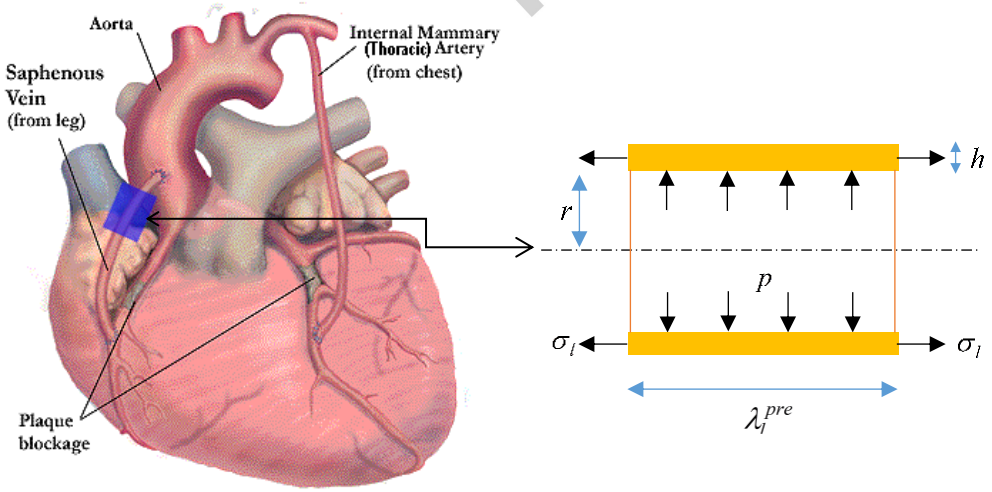


Fig. 3 A thin-walled vessel model for GSV. The heart picture is from [38].

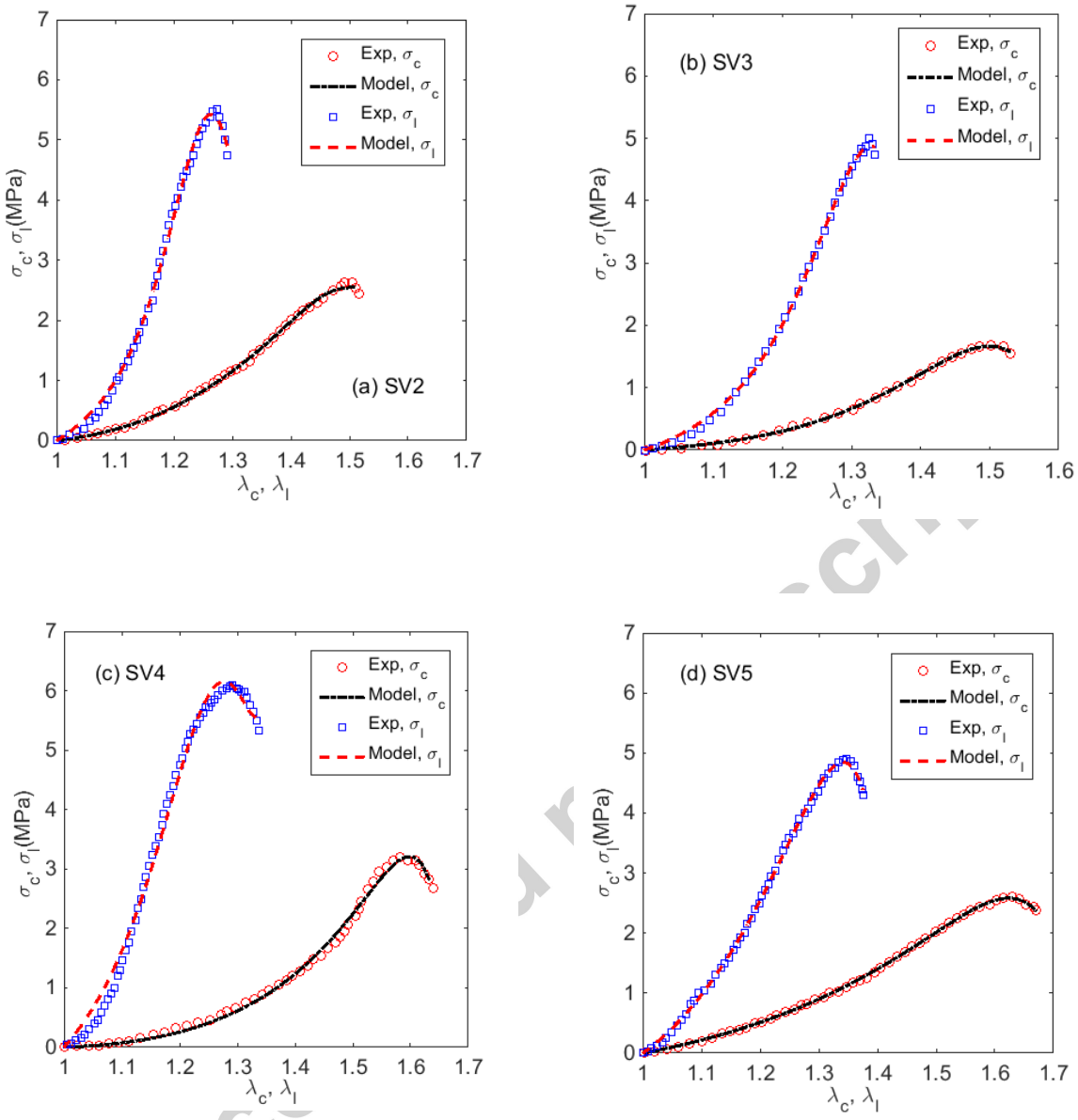


Fig. 4 The stress-stretch curves predicted with extracted model constants against the experimental stress-stretch curves for four GSVs SV2-5

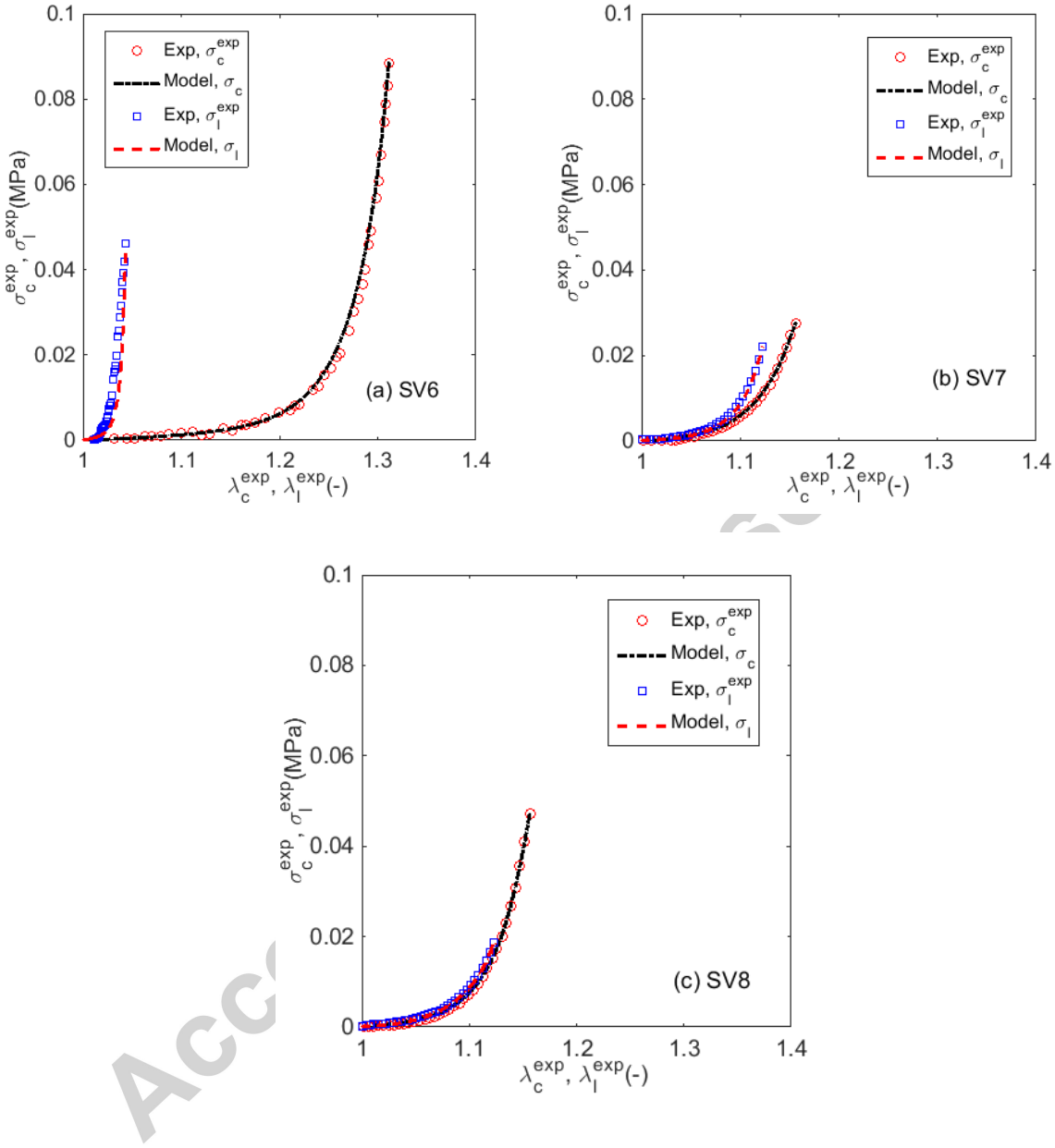


Fig. 5 The stress-stretch curves predicted with extracted model constants for GSV samples SV6, 7 and 8 against their tested data, SV6 from [31], SV7 and 8 from [30].

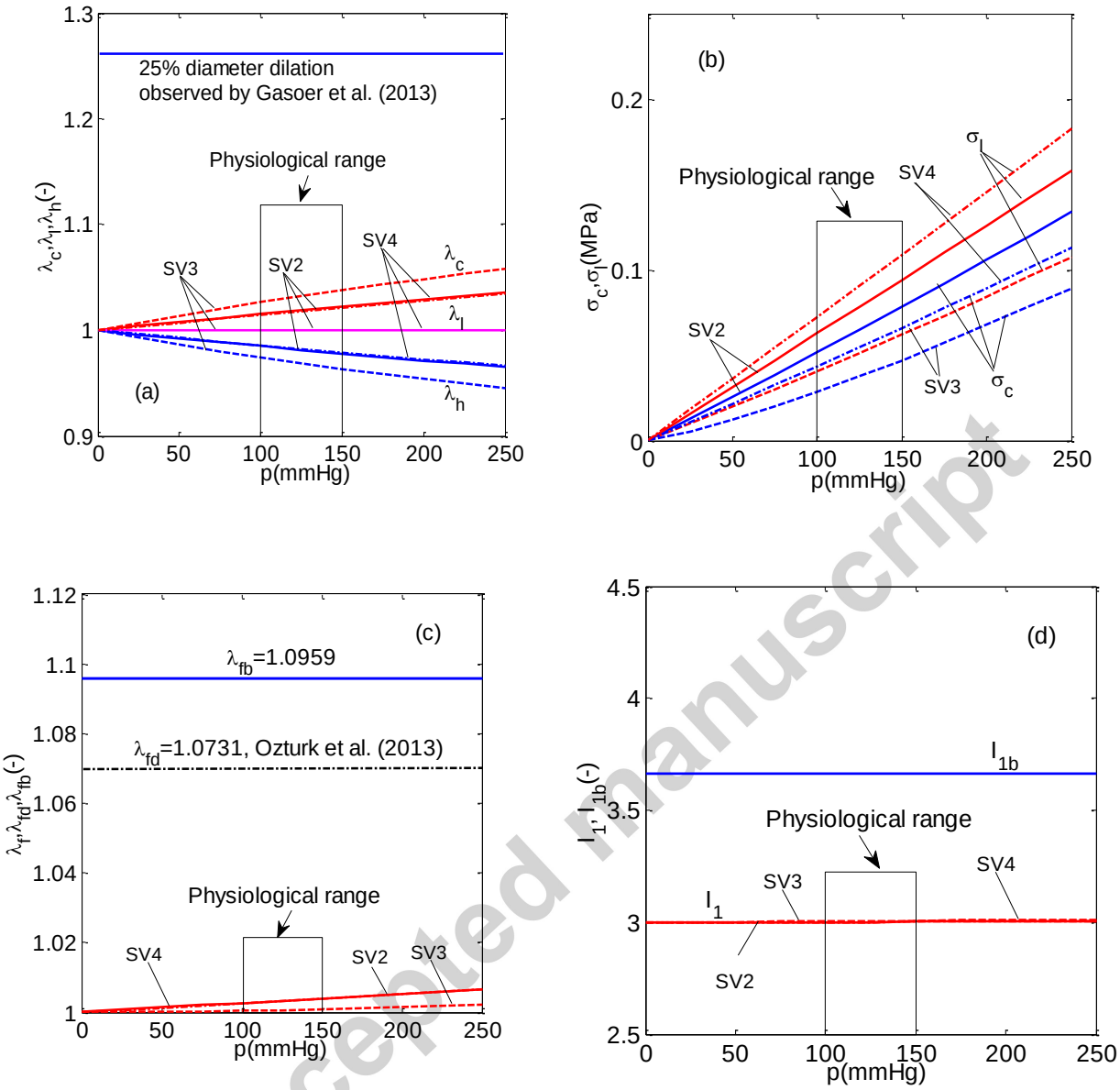


Fig. 6 The predicted vessel stretch (a), stress (b), fibre stretch (c) and invariant $I_1$ (d) curves in response to a variable internal blood pressure for SV2, 3 and 4 under coronary artery physiological condition.

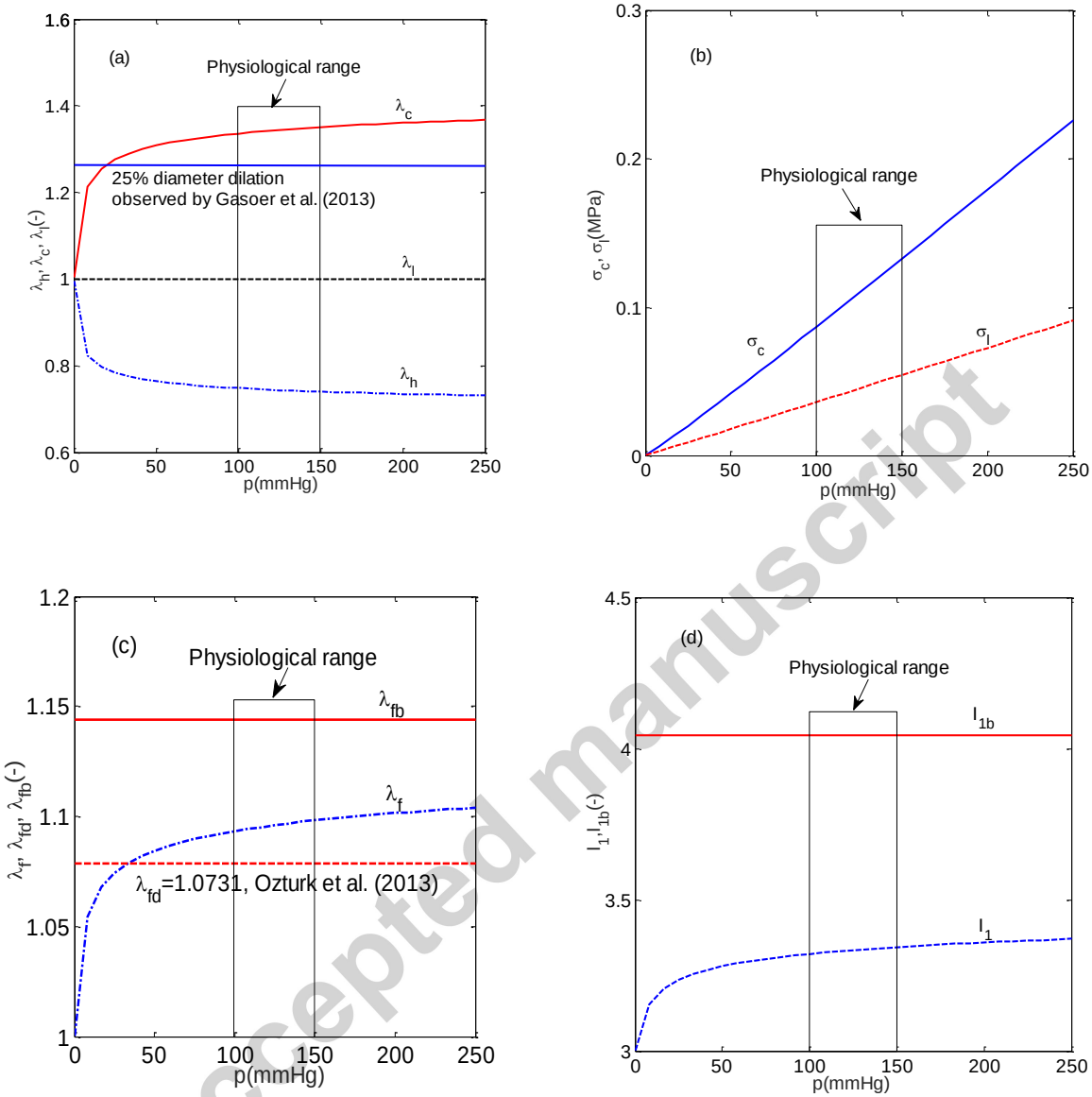




Fig. 7 The predicted vessel stretch (a), stress (b), fibre stretch (c) and invariant $I_1$ 9(d) curves in response to a variable internal blood pressure for SV6 under coronary artery physiological condition.

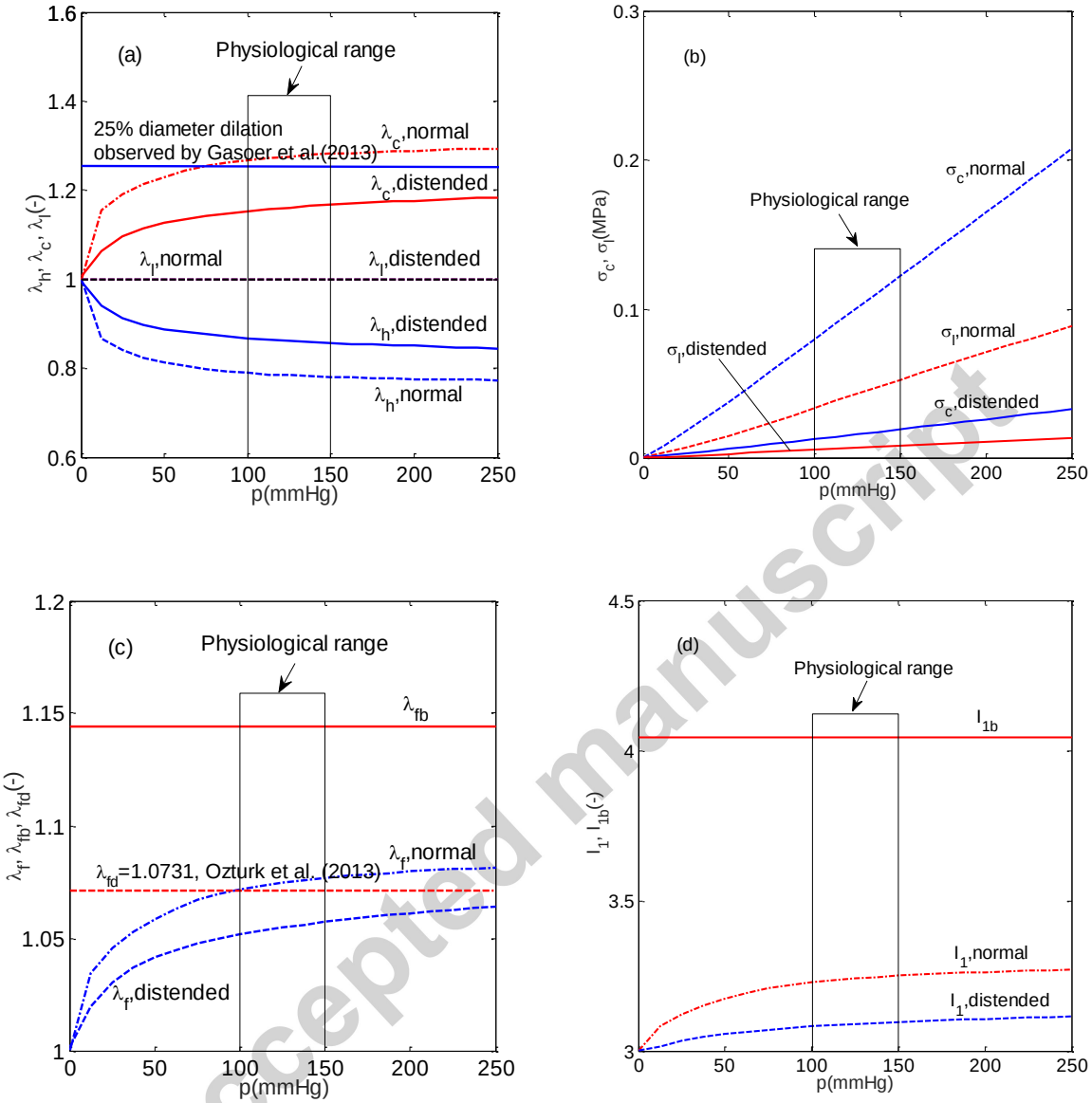


Fig. 8 The predicted vessel stretch (a), stress (b), fibre stretch (c) and invariant $I_1$ (d) curves in response to a variable internal blood pressure for SV7 (normal) and 8 (distended) under coronary artery physiological condition.

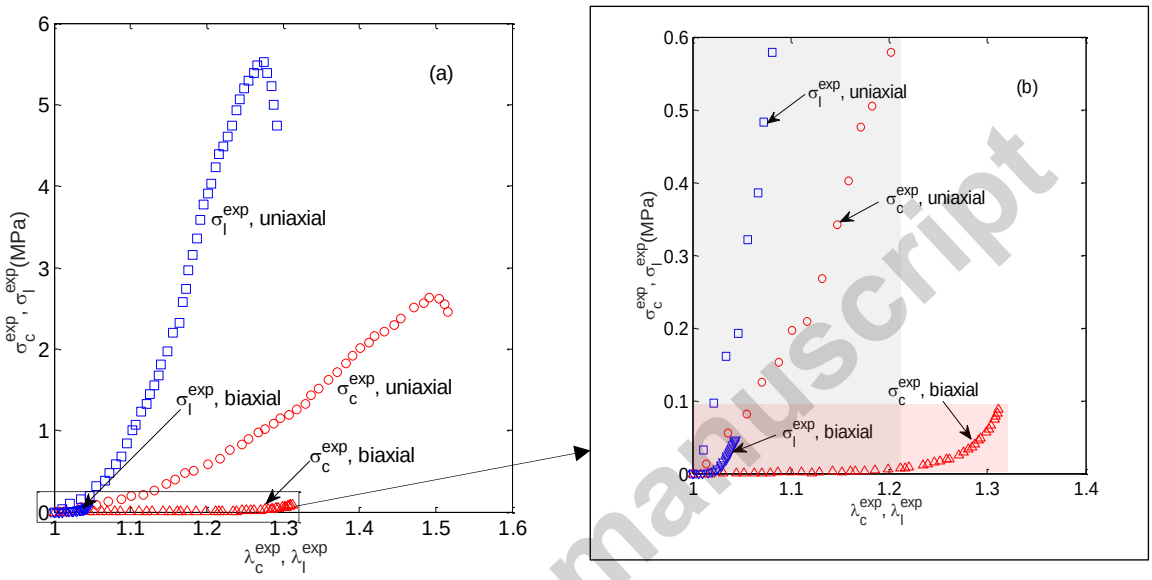


Fig. 9 A comparison of stress-stretch region and curve shape between uniaxial tensile test on SV2 and tubular biaxial inflation test on SV6.